



# The Mogangling giant landslide triggered by the 1786 Moxi M 7.75 earthquake, China

Bo Zhao<sup>1,2</sup> · Yunsheng Wang<sup>2</sup> · Junfeng Wu<sup>3</sup> · Lijun Su<sup>1,4,5,6</sup> · Jiangwei Liu<sup>2</sup> · Gang Jin<sup>2</sup>

Received: 15 June 2020 / Accepted: 9 December 2020 / Published online: 2 January 2021  
© The Author(s), under exclusive licence to Springer Nature B.V. part of Springer Nature 2021

## Abstract

A good understanding of seismic giant landslides could provide favourable guidance for seismic stability evaluation of nearby slopes. Here, an excellent example of a catastrophic seismic landslide named the Mogangling giant landslide (MGL), located upstream along the Dadu River and triggered by the 1786 Moxi M 7.75 earthquake, is analysed for its deposit characteristics, failure mechanism and dammed lake. The MGL, with a volume of approximately  $4500 \times 10^4 \text{ m}^3$ , 450 m long and 1000 m wide, blocked the Dadu River completely and caused over 100 000 deaths when the landslide dam broke. The MGL occurred on the upper part of a narrow granite ridge; a potentially unstable wedge-shaped rock mass was separated from the remaining massif by unloading fissures and an active fault (Detuo fault) that just crossed the slope foot. The Moxi earthquake coupled with strong site amplification triggered the MGL, which blocked the Dadu River; the elevation of the dam crest was approximately 130 m higher than the present river level. The dammed lake had a volume of approximately  $9.504 \times 10^8 \text{ m}^3$ , an area of 19.91 km<sup>2</sup> and a length of approximately 31 km; the peak flow of the outburst flood was larger than 7100 m<sup>3</sup>/s. After hundreds of years of concave bank erosion, the deposit is divided into the right bank deposit (main deposit) and left bank deposit (residual deposit).

**Keywords** Mogangling giant landslide (MGL) · 1786 Moxi M 7.75 earthquake · Failure mechanism · Dammed lake

---

✉ Bo Zhao  
zhaobo1989@imde.ac.cn

✉ Yunsheng Wang  
wangys60@163.com

<sup>1</sup> Key Laboratory of Mountain Hazards and Earth Surface Processes, and Institute of Mountain Hazards and Environment, Chinese Academy of Sciences, Chengdu 610041, China

<sup>2</sup> State Key Laboratory of Geohazard Prevention and Geoenvironment Protection, Chengdu University of Technology, Chengdu 610059, China

<sup>3</sup> Architecture and Art College, Yiwu Industrial and Commercial College, Yiwu 322000, China

<sup>4</sup> CAS Center for Excellence in Tibetan Plateau Earth Sciences, Beijing 100101, China

<sup>5</sup> China-Pakistan Joint Research Center On Earth Sciences, Islamabad, Pakistan

<sup>6</sup> University of Chinese Academy of Sciences, Beijing 100049, China

## 1 Introduction

Seismic giant landslides refer to seismic landslides with volumes  $\geq 10^6 \text{ m}^3$  and are important drivers of regional landscape evolution and erosion rates (Turnbull and Davies 2006; Korup et al. 2007; Hewitt et al. 2008; Antinao and Gosse 2009; Pánek et al. 2010). Seismic giant landslides usually affect slopes at depths of tens to hundreds of metres of terrain change under strong seismic shaking, and sudden dramatic terrain changes can have catastrophic consequences, such as blocking rivers and burying villages (Dai et al. 2005; Chen et al. 2013; Guo et al. 2016; Deng et al. 2017; Wang et al. 2018a).

At present, giant seismic landslides occur all around the world (Petley 2013; Havenith 2014; Yang et al. 2014; Kargel et al. 2016), and the eastern margin of the Tibetan Plateau (EMTP) is a typical area prone to seismic giant landslides (Dai et al. 2005; Huang and Fan 2013; Guo et al. 2016; Wu et al. 2018; Wang et al. 2018b). The EMTP, forming the transitional zone between the Tibetan Plateau and the Sichuan Basin, presents strong tectonic activity, high geostress, frequent mega-earthquakes and intense river erosion; these unfavourable factors make this region a world famous area prone to seismic giant landslides. For example, the 2008 Wenchuan Ms 8.0 earthquake triggered 112 giant landslides (Xu et al. 2009a, b, 2011); the 1933 Diexi Ms 7.5 earthquake generated 17 giant landslides, (Zhao 2020); the 1879 Wenxian Ms 8.0 earthquake produced 49 giant landslides; and the 1786 Moxi Ms 7.75 earthquake triggered at least 3 giant landslides (Wang et al. 2019; Zhao 2020). The typical geomorphic features of deeply cut gorges in the EMTP give these seismic giant landslides, such as the Tangjiashang landslide, Daguangbao landslide, Lantianwan landslide and Wangjiayan landslide, the characteristics of high source relief, completely dammed rivers and bedrock outcrops that appear deceptively stable due to incomplete disintegration (Cui et al. 2012; Huang et al. 2012; Yin et al. 2015; Wang et al. 2019).

In fact, a seismic giant landslide is the important beginning of a hazard chain and is responsible for the next blockage of a river or frequent debris flows (Xu et al. 2009a, Huang and Fan 2013, Wang et al. 2019, Zhao et al. 2019). A good understanding of the failure mechanism and damming process could provide useful guidance for interrupting hazard chains and evaluating regional susceptibility. In this study, we present an example of an ancient seismic giant landslide—the Mogangling giant landslide (MGL) triggered by the 1786 Moxi M 7.75 earthquake, located in the upstream reach of the Dadu River. The Dadu River is a typical active river, and numerous giant landslides are distributed along its bank (Wu et al. 2011; Wang et al. 2012, 2019; Deng et al. 2017). According to historical records, the MGL dam blocked the Dadu River completely, and the breaching of the landslide dam 10 days after the occurrence of the landslide caused more than 100 000 deaths in the downstream section (Dai et al. 2005; Wu et al. 2013).

The main objectives of this study are to (1) analyse the regional setting, morphological features and typical characteristics of the source area and deposit area; (2) determine the failure mechanism; and (3) discuss the process of dam break.

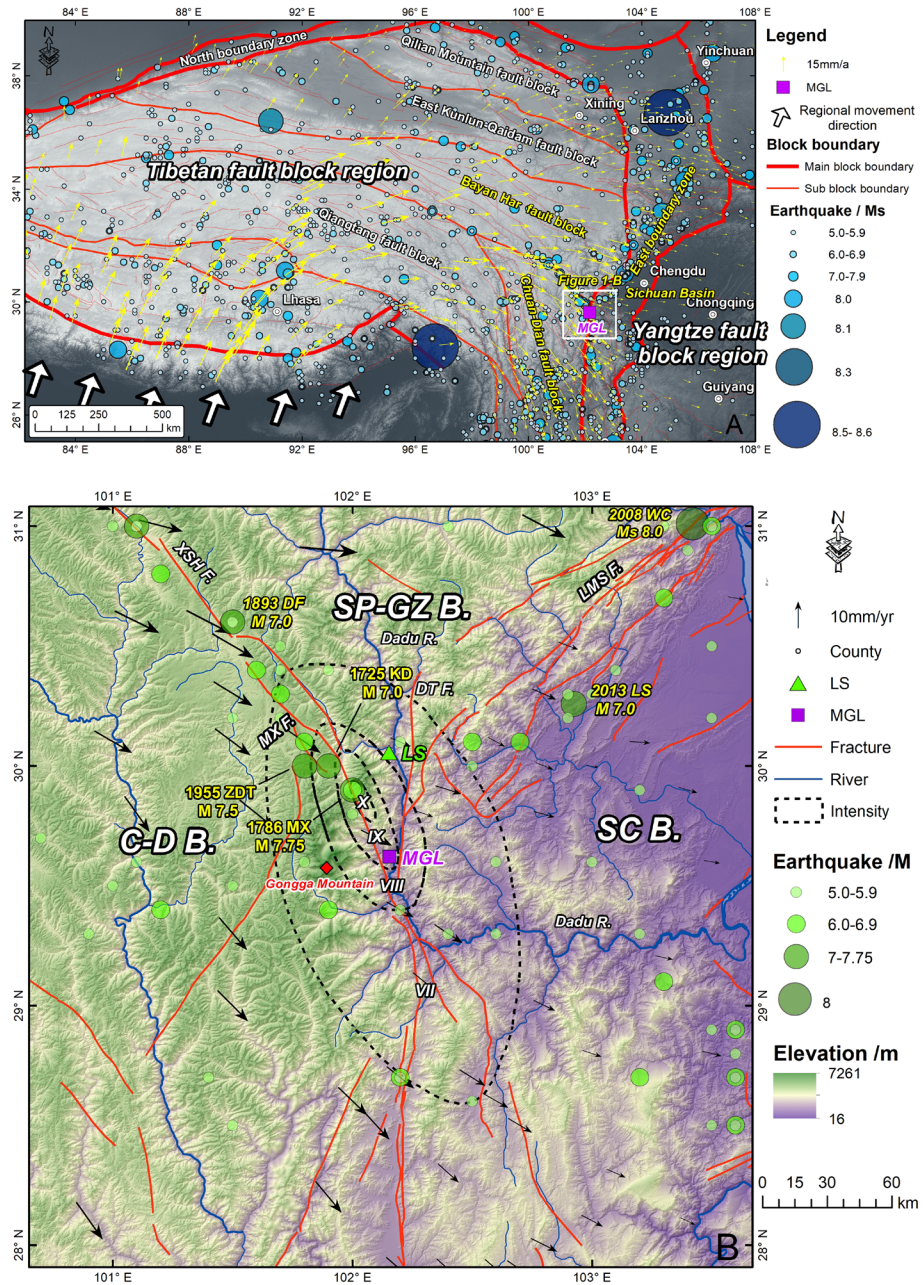


**Fig. 1** Location and regional tectonic settings of MGL landslide. **a** Large regional tectonic and seismic features and landslide location, **b** distribution of sub-fault blocks, historical earthquakes, fault zones and topography features around landslide site and seismic intensity of Moxi earthquake. The historical earthquakes are from China Earthquake Network Center (<http://www.cenc.ac.cn/>), the GPS data are from Zhao et al. 2015, intensity contour of Moxi earthquake is from Dai et al. 2005. *SC B* Sichuan basin, *C-D B* Chuan-Dian block, *SP-GZ B* Songpan-Ganzi block; *KD* Kangding (earthquake), *LS* Lushan (earthquake), *MX* Moxi (earthquake), *ZDT* Zhedutang (earthquake), *DF* Daofu (earthquake), *WC* Wenchuan (earthquake); *LMS F*. Longmenshan fault zone, *XSH F*. Xianshuhe fault zone, *DT F*. Detuo Fault zone. *LS* Lengzhuguan station, *MGL* Mogangling giant landslide

## 2 Geomorphic and geological setting

### 2.1 Regional tectonic setting

The MGL is located in Mogangling Mountain, Luding County, Sichuan Province, Southwest China, which is on the EMTP (Fig. 1a). The EMTP is a transitional zone between the Tibetan fault block and the Yangtze fault block and is famous for its widespread tectonic activity and earthquakes (Hubbard and Shaw 2009; Xu et al. 2017; Ren et al. 2018). The MGL lies in one of the areas with the most active tectonism (Fig. 1a).

According to regional tectonic structures, the MGL area is at the intersection of 3 blocks separated by active fault zones: the Sichuan Basin, Songpan-Ganzi block (eastern margin of the Baryan Har fault block in Fig. 1a) and Chuan-Dian block; numerous earthquakes are distributed along block boundaries (Fig. 1b; Wang et al. 2011; Sun et al. 2018). Regional global positioning system (GPS) measurements near the MGL area present an obvious change from more than 10 mm/y in the Chuan-Dian block decreasing to less than 6 mm/y in the Sichuan Basin (Fig. 1b, Zhao et al. 2015); much strain energy accumulates here, and high geostress is widely distributed (Wu et al. 2013).

Two fault zones also meet near the MGL area: (1) the Longmenshan fault zone that triggered the 2008 Wenchuan Ms 8.0 and 2013 Lushan Ms 7.0 earthquakes (Xu et al. 2009a, b; Gorum et al. 2011; Xu et al. 2013b) and (2) the Xianshuihe fault zone that has produced numerous large earthquakes, such as the 1725 Kangding Ms 7.0, 1786 Moxi Ms 7.75 and 1955 Zheduotang Ms 7.5 earthquakes (Zhou et al. 1983; Papadimitriou et al. 2004; Dai et al. 2005; Fig. 1b).

The MGL is in the upstream reach of the Dadu River and on the right river bank (Figs. 1b, 2). The high relief from more than 7000 m (Gongga Mountain in Fig. 1b) to less than 1000 m (Dadu River valley) and the deeply cut gorge are typical geomorphic features of the MGL area. Four sub-faults, the Moxi fault, Detuo fault, Maowen fault and Jinping fault, converge in the MGL area (Fig. 2); these sub-faults are branches of the Longmenshan fault zone (Maonian fault) and Xianshuihe fault zone (Moxi fault, Detuo fault and Jinping fault) (Zhao et al. 2012; Wu 2013; Qi et al. 2017).

The MGL area is an area with typically high geostress; the maximum principal stress reaches 26 MPa and is oriented in the N50°–75°W direction (Huang et al. 2011; Wu 2013). This stress and the rapid river incision (Luding section: 0.38 mm/y, Zhao et al. 2013) causes rock to unload strongly towards the free space. All these factors lead to many fractures in the rocks near the MGL area (Wang et al. 2007). Frequent earthquakes can easily trigger these fractured rocks, making the MGL area susceptible to large landslides, as shown in Fig. 2. Based on field investigations, there are 17 giant landslides distributed along the Luding section of the Dadu River (approximately 65 km long); detailed information on these giant landslides is listed in Table 1. All these palaeo-landslides blocked the Dadu River, and the MGL is one of the youngest.

On 1 June 1786, a very large earthquake (the Moxi earthquake) struck the Luding area with an epicentre located at 101° 15' E, 30° 03' N and a focal depth of approximately 20 km (Wang and Pei 1988; Dai et al. 2005). Its magnitude is estimated at  $M=7.75$ , its surface rupture extended approximately 80 km, and its intensity reached degree X, as shown in Fig. 2 (Wang and Pei 1988). The seismogenic fault is the Moxi fault, which is a thrust and sinistral strike-slip fault with an average horizontal slip rate of  $9.9 \pm 0.6$  mm/y (Zhou et al. 2001; Dai et al. 2005). The MGL is located in the hanging wall area of the Moxi seismic event within the intensity IX area (Fig. 2).

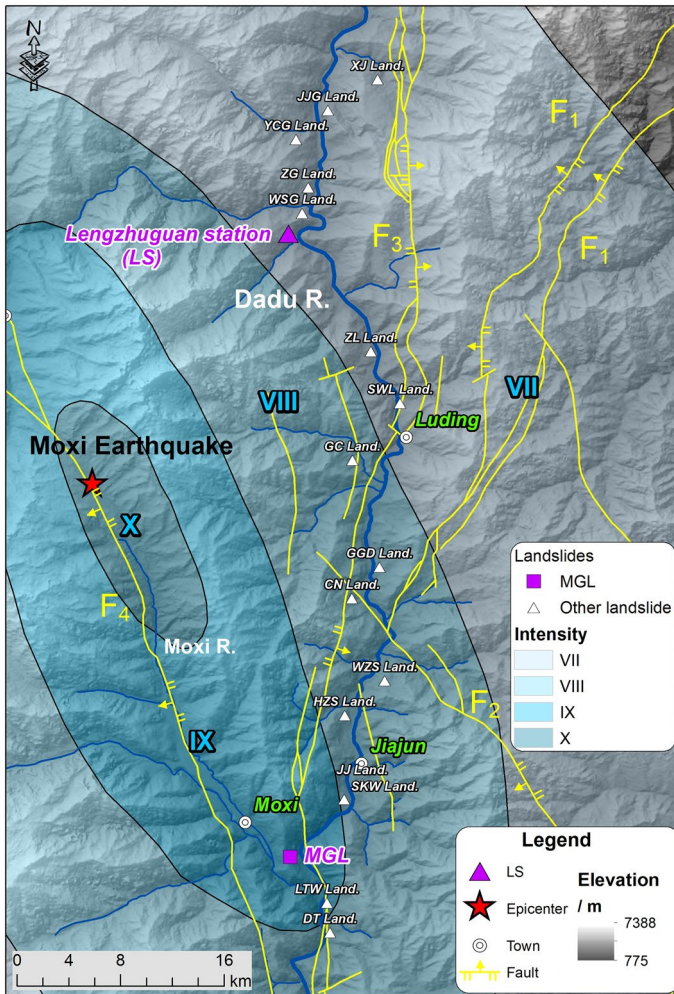


**Fig. 2** Small regional settings around MGL and distribution of nearby giant landslides. *F1*–Maowen fault (Longmenshan fault zone), *F2*–Jinping fault, *F3*–Detuo (DT) fault, *F4*–Moxi fault. The detail information of giant landslides is listed in Table 1. The intensity is the intensity contour of 1786 Moxi earthquake (Dai et al. 2005)

The Moxi earthquake triggered at least 3 giant landslides: the Mogangling, Lantianwan and Detuo landslides, as listed in Table 1 (Wu 2013; Gu et al. 2016; Wang et al. 2019). The Mogangling landslide was the most serious slide; it blocked the Dadu River and later caused more than 100 000 deaths when the landslide dam broke (Dai et al. 2005).

## 2.2 Geomorphic and lithological features

Figure 3 shows a geological map of the MGL area, which is mainly composed of intrusive rocks (granite and diorite), the Triassic Xujiage Group and Quaternary sediments. The granite can be divided into common granite ( $\gamma_2$ ), potash feldspar granite ( $\gamma_{k2}$ ), plagiogranite

**Table 1** Detail information of giant landslides in Dadu River Luding section

Landslide	Scale (10 <sup>6</sup> m <sup>3</sup> )	Type	Location		Block river	River bank	Occurred time
			E (°)	N (°)			
Gancaocun (GC)	880	Rock	102° 11' 50"	29° 53' 55"	Yes	Right	Ancient
Detuo (DT)	4.3	Rock	102° 10' 54"	29° 34' 12"	Yes	Left	Ancient
Lantianwan (LTW)	30	Rock	102° 10' 46"	29° 35' 27"	Yes	Left	1786
Mogangling (MGL)	45	Rock	102° 09' 41"	29° 37' 30"	Yes	Right	1786
Jiajun (JJ)	130	Rock	102° 12' 15"	29° 40' 26"	Yes	Left	Ancient
Shangkuiwu (SKW)	55	Rock	102° 11' 30"	29° 39' 47"	Yes	Right	Ancient
Haizishang (HZS)	15	Rock	102° 11' 32"	29° 43' 17"	Yes	Right	Ancient
Wuzhisuo (WZS)	200	Rock	102° 13' 11"	29° 44' 43"	Yes	Left	Ancient
Gangudi (GGD)	380	Rock	102° 12' 58"	29° 49' 28"	Yes	Left	Ancient
Chuni (CN)	400	Rock	102° 21' 1"	29° 49' 20"	Yes	Right	Ancient
Siwanli (SWL)	50	Rock	102° 13' 49"	29° 56' 18"	Yes	Left	Ancient
Zanli (ZL)	30	Rock	102° 12' 37"	29° 58' 28"	Yes	Right	Ancient
Wasigou (WSG)	190	Rock	102° 9' 51"	30° 4' 21.89"	Yes	Right	Ancient
Zhanggu (ZG)	290	Rock	102° 10' 3"	30° 5' 20"	Yes	Right	Ancient
Yangchangu (YCG)	1.1	Rock	102° 10' 18"	30° 7' 58"	Yes	Right	Ancient
Jiaojigou (JJG)	5.8	Rock	102° 11' 6"	30° 5' 10"	Yes	Left	Ancient
Xiongju (XJ)	2.0	Rock	102° 10' 3"	30° 5' 20"	Yes	Left	Ancient
Ganhaizi (GHZ)	16	Rock	101° 52' 38"	30° 57' 18"	Yes	Right	Ancient

( $\gamma_{02}$ ) and migmatitic granite ( $\gamma_{M2}$ ). The MGL occurred in the plagiogranite ( $\gamma_{02}$ ), and some outcrops of the Triassic Xujiache Group are present on the bank opposite the MGL (Fig. 3). The Detuo fault, especially its western branch, crosses the MGL (Fig. 3).

The MGL originated on a typical narrow ridge bounded by two rivers: the Dadu River and the Moxi River (Fig. 4). The Dadu River has an obvious deflection at the MGL, where it turns from NE in the upstream reach to SE in the downstream reach. The concave bank erosion theory (Page and Nanson 1982; Nanson and Hickin 1986) indicates that the foot of Mogangling Mountain is continuously eroded. The Dadu River is an important tributary of the Yangtze River; the maximum discharge generally occurs during the summer season between June and September, the flow is between 100 and 1500 m<sup>3</sup>/s, and the average flow is approximately 891 m<sup>3</sup>/s (Dai et al. 2005).

The high geostress and intense rock unloading have fractured Mogangling Mountain; for example, two outcrops of very fractured rocks collapse frequently (Fig. 4c, d).

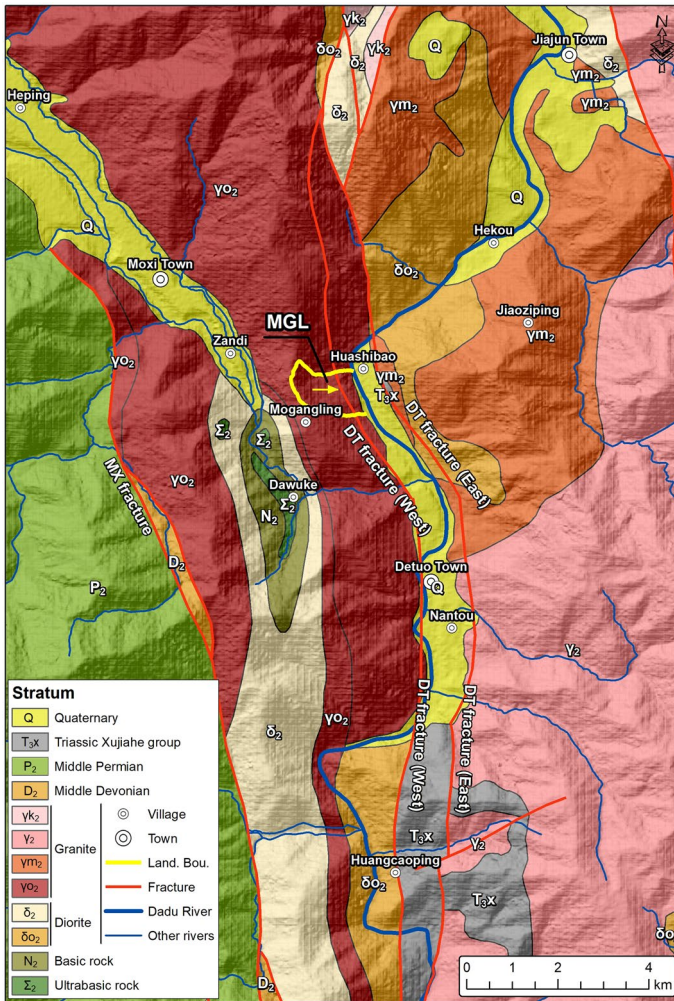
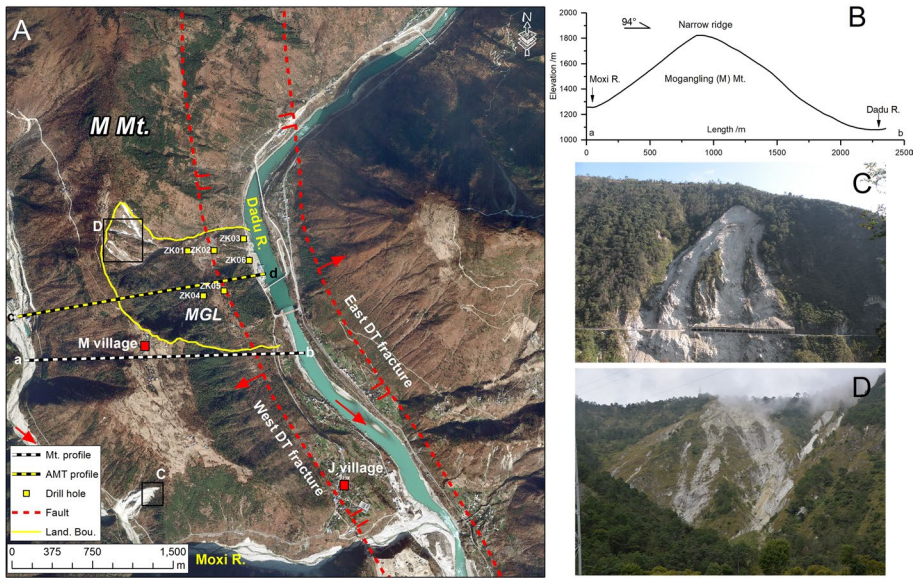


Fig. 3 Geological map around MGL landslide. The geological data are from CIGMR (1975)

This situation poses a serious threat to traffic safety and provides sufficient deposits for the occurrence of debris flows.

### 3 Methodology

In this study, a detailed field investigation, along with unmanned aerial vehicle (UAV) and digital photography, drill holes, geophysical prospecting, historical records and seismic responses, is used to study the geomorphic features, deposit structure and zonation, failure mechanism and dammed lake caused by the MGL.



**Fig. 4** Typical characteristics of M (Mogangling) mountain. **a** Satellite image of Mogangling landslide, **b** profile of Mogangling mountain, **c–d** field photographs of fractured rock at c point and d point. Geophysical prospecting profile (c–d) is shown in Fig. 8. The satellite image is from Google earth

### 3.1 Field investigation and drill holes

A detailed field investigation was conducted using a hand-held GPS instrument, laser rangefinders, geological compass and field records. The material composition, boundaries and other field properties of the landslide deposits were determined and recorded. The slope structures, the lithology of the source area and evidence of the failure mechanism were also collected. UAVs were used to characterize the overall features of the MGL. Historical records about the MGL were gathered to identify the triggering factor and the features of the dammed lake. A high-resolution topographic map (1:5 000), geological map (1:200 000), and detailed parameters for the Moxi earthquake are also obtained.

**Table 2** Detail information of 6 drill holes

Drill hole	Location		Elevation (m)	Drilling depth (m)	Deposit depth (m)
	E (°)	N (°)			
ZK01	102.156262	29.62522	1375	97.30	97.30
ZK02	102.158472	29.62525	1335	202.10	192.00
ZK03	102.160950	29.62611	1125	96.20	15.60
ZK04	102.157582	29.62195	1400	103.50	79.10
ZK05	102.159298	29.62231	1355	202.90	180.70
ZK06	102.161417	29.62454	1145	95.10	85.20



Six drill cores (Fig. 9, Table 2), whose lengths ranged from 95 to 202 m, were drilled to characterize the deposit structures and depths, the original river channel, the bedrock and the scale of the landslide. Detailed information about the 6 drill holes is listed in Table 2.

### 3.2 Geophysical prospecting profile

To clarify the internal characteristics of the MGL, a geophysical prospecting profile (Fig. 4a) using the audio-frequency magnetotelluric (AMT) method was measured, and the geophysical prospecting equipment used was a V8 Electric instrument (Canadian Phoenix Geophysics, <http://www.phoenix-geophysics.com/products/receivers/v8/>). The location of the geophysical prospecting line is shown in Fig. 4a; its length was 2000 m, and the interval between adjacent sounding points was 20 m. The standard crisscross pole distribution was adopted as shown in Fig. 5.

The sounding depth can be estimated by the following equation (Liu 2014).

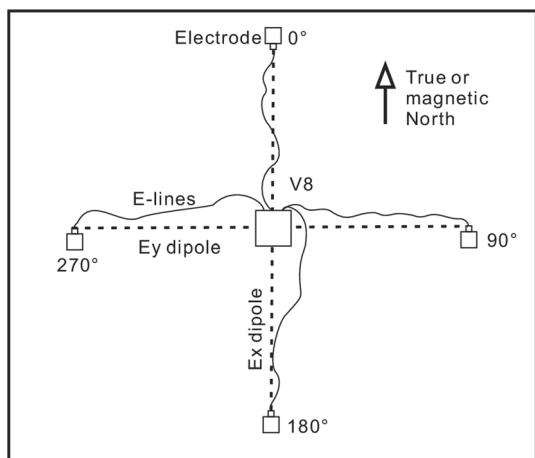
$$h = 365 \sqrt{\rho_s / f} \quad (1)$$

where  $h$  is the estimated prospecting depth,  $\rho_s$  is the resistivity and  $f$  is the frequency. The frequency range of the V8 system, was 0.1–10,000 Hz, and the sounding depth could range from tens of metres to thousands of metres (Zhang 2015). The MTSOFT2D software was adopted for lateral data processing and inversion, and the inversion was performed by the Bostick method. The interpreted result is shown in Fig. 8.

### 3.3 Seismic response to narrow ridge

The MGL was triggered by an M 7.75 earthquake (the Moxi event), and the seismic conditions of the Mogangling slope instability can provide useful guidance for determining the failure mechanism. Therefore, a simple earthquake station, named the Lengzhuguan (LZG) station, was established 50 km upstream from the MGL (Figs. 1b, 2) in a location with features similar to those of the MGL, including corresponding geomorphic units (narrow ridge linked to a large mountain and cut by two rivers) and the same lithology (granite); both locations are on the right river bank and have a concave bank (Figs. 3, 4a, 6a).

**Fig. 5** Standard crisscross pole distribution of sounding points using AMT method. The figure is revised from Liu (2014)



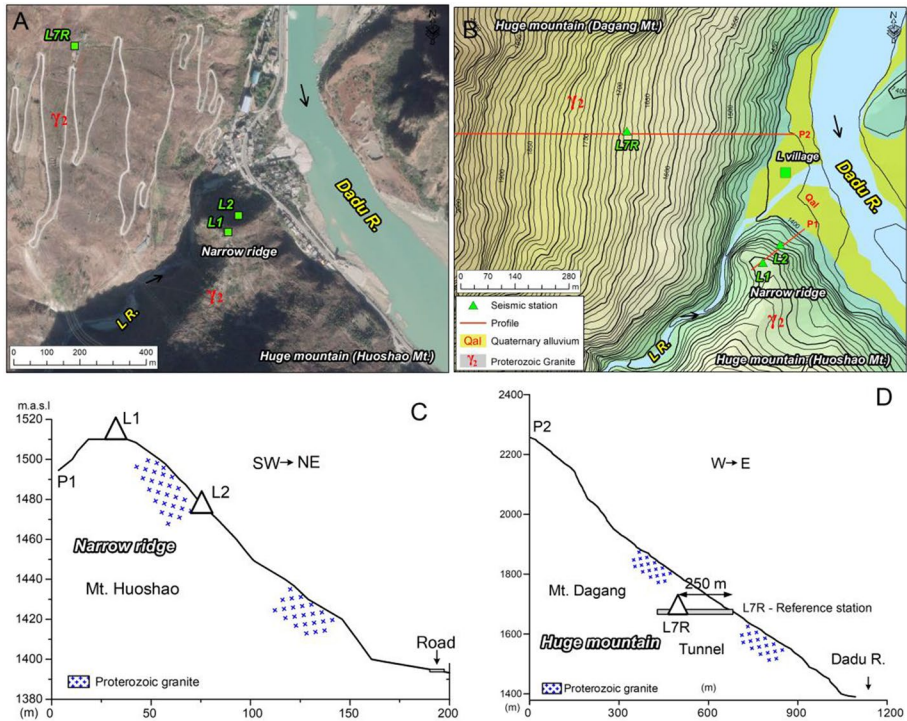


**Fig. 6** Layout of Luzhuguan seismic station. **a–b** Accelerometers distribution from satellite image and topographic map, **c** profile section of accelerometer L1 and L2, **d** profile section of accelerometer L7R (reference station). Satellite image is from Google earth

The LZG station, made up of 3 accelerometers, is located on a narrow granite ridge (L1 and L2), as shown in Fig. 6. Because the MGL occurred in the upper part of the narrow ridge, accelerometers L1 and L2 are located in the middle and top parts of the narrow ridge, and accelerometer L7R is in the inner part (250 m) of the large mountain and treated as a reference station. The Lengzhuguan station works year round to capture as many seismic events as possible.

#### 4 Moxi earthquake triggered the MGL

At noon on 1 June 1786, the Moxi M 7.75 earthquake struck the Luding area and triggered the MGL, which was recorded on a local stele (Fig. 7a). The distance from the MGL to the epicentre is approximately 31 km, while that to the seismic fault (Moxi fault) is only approximately 2 km.

The main slide direction is approximately  $75^\circ$ . After hundreds of years of erosion and transformation, some deep gullies have formed, especial at its two lateral boundaries (downstream boundary and upstream boundary, Figs. 7, 9). The front edge of the deposit is the Dadu River, the deposits have been eroded intensively (Fig. 7e), and obvious local headscarps exist (Fig. 9).

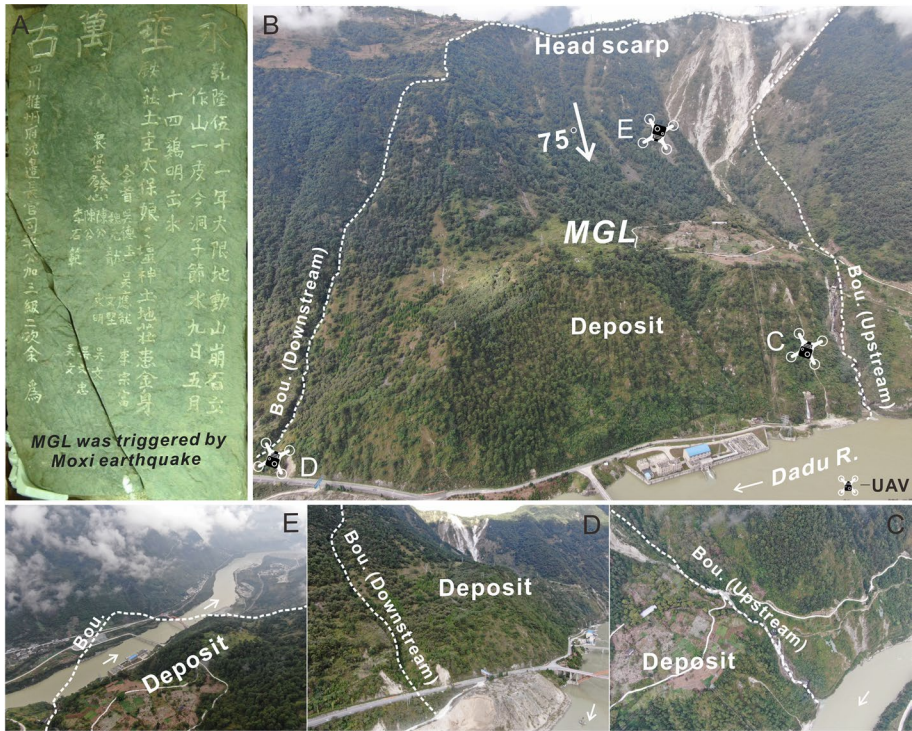


**Fig. 7** Overall UAV images of MGL. **a** Moxi earthquake-triggered MGL recorded by ancient stele, **b** overall UAV images of MGL, **c** upstream boundary, **d** downstream boundary, **e** front edge of MGL

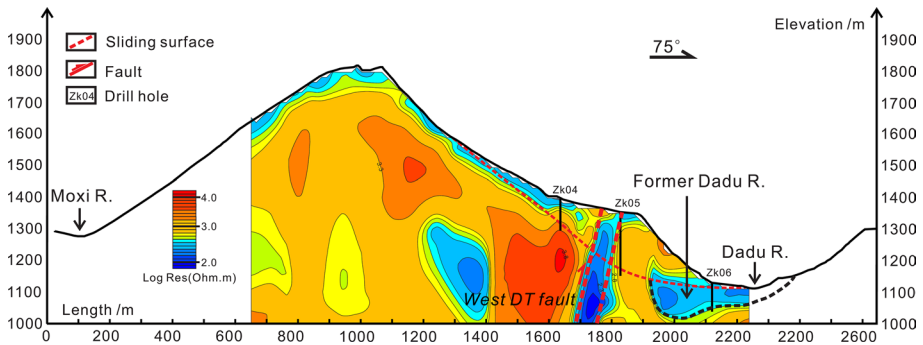


**Fig. 8** Geophysical prospecting profile (AMT method) of Mogangling landslide; location of profile is shown in Fig. 4a

The interpreted results of geophysical prospecting using the audio-frequency magnetotelluric (AMT) method are shown in Fig. 8. Figure 8 illustrates that the Detuo fault just crosses the slope foot, which may have had a direct influence on the occurrence of the MGL. The original course of the Dadu River was also located at the original slope foot, and the MGL forced the channel eastward (Figs. 8, 10).

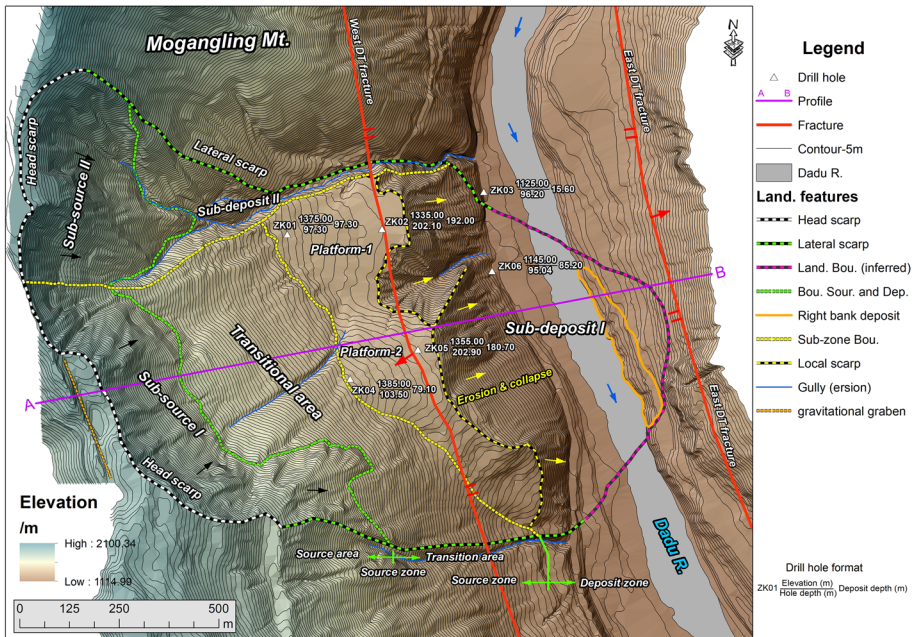


Fig. 9 Topographic features of Mogangling landslide

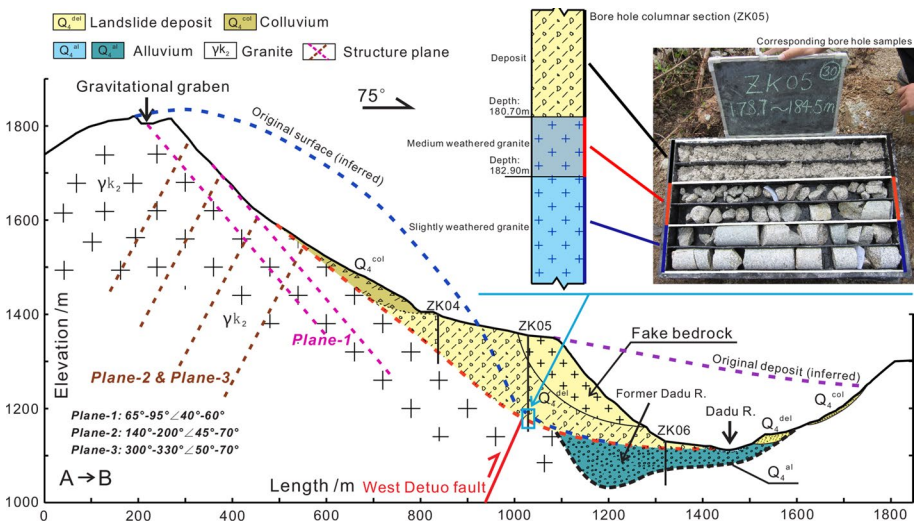


Fig. 10 Geological profile of Mogangling landslide; location of profile is listed in Fig. 9. Structure plane-1 is bedding plane, structure plane-2 and structure plane-3 are lateral planes

The width (along the river), length and relative height of the MGL are approximately 1000 m, 1200 m and 770 m, respectively (Figs. 9, 10), and the deposit depth varies between 55 and 192 m, as revealed by drill holes (Fig. 9). The volume of the MGL is approximately  $4500 \times 10^4 \text{ m}^3$ .

After the occurrence of the MGL, its deposits blocked the Dadu River (Fig. 9), and 10 days after the event occurred, the dam broke (Dai et al. 2005). An obvious residual deposit platform remains in the front section (Figs. 9, 10), which indicates that the deposits accumulated at the bottom of the V-shaped gorge and completely filled it after the unstable slope broke loose; a relatively gentle platform formed, which is similar to the Tangjiashan landslide deposit triggered by the 2008 Wenchuan earthquake (Xu et al. 2013a). The rock in the source zone is plagiogranite, and the boundary between the deposit zone and source zone is clear (Fig. 11). Hundreds of years of erosion have completely cut the deposits into 2 parts (right bank part and left bank part), as shown in Fig. 11.

### 5 Landslide zonation and corresponding characteristics

According to the field investigations, in addition to dividing the MGL into the source zone and the deposit zone, each zone be divided into sub-zones. The deposit zone is divided into 2 sub-zones (sub-deposits I and II). The source zone can be divided into the source area and the transitional area; the source area can also be divided into 2 sub-sources (sub-sources I and II), as shown in Fig. 11. These sub-zones feature different morphological elements and geological structures and are discussed in detail.

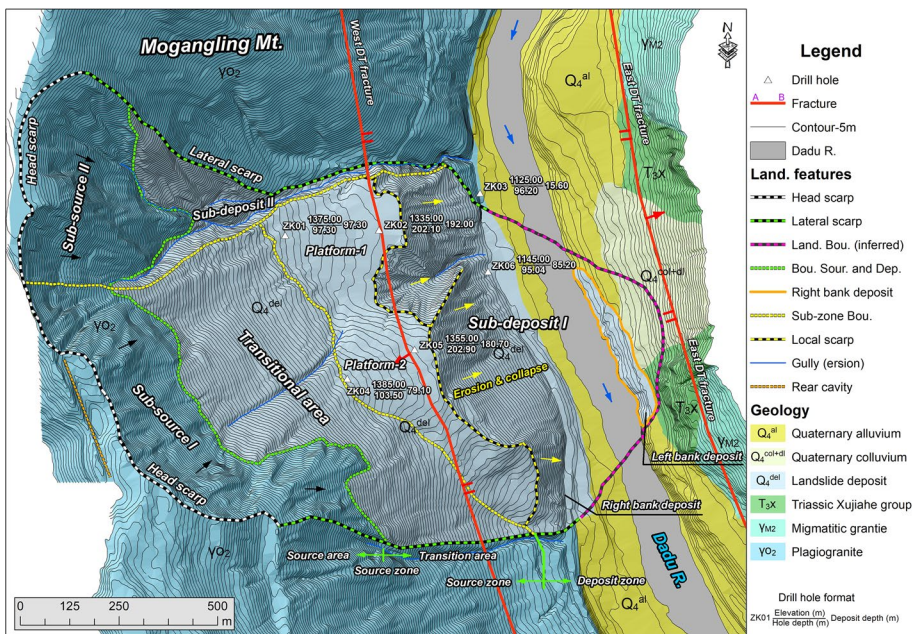


**Fig. 11** Geological features and sub-zones of MGL. Geological data are from field investigation and CIGMR (1975)

## 5.1 Source zone

The elevation in the source zone varies between 1380 and 1890 m. The bedrock of the MGL is plagiogranite, which is an intrusive rock without internal planes; thus, the structural planes that developed in the rock mass become the key element to slope stability. According to numerous structural plane measurements in the source zone, 3 obvious sets of structure planes are present: plane-1:  $65^{\circ} - 95^{\circ} \angle 40^{\circ} - 60^{\circ}$ , plane-2:  $140^{\circ} - 180^{\circ} \angle 45^{\circ} - 70^{\circ}$ , and plane-3:  $300^{\circ} - 330^{\circ} \angle 50^{\circ} - 70^{\circ}$ . The corresponding stereographic projection indicates a potential wedge-shaped rock mass bounded by these sets of structure planes (Fig. 12a). Plane-1 is a bedding plane, and plane-2 and plane-3 are lateral planes (Fig. 10). Numerous wedge-shaped rock masses (Fig. 12b, c) and small wedge failures (Fig. 12d) are formed by these sets of structural planes in the source zone. These results indicate that the MGL is a wedge-shaped rock mass failure landslide.

The source zone can be divided into the source area (1600–1890 m in elevation) and the transitional area (1380 m–1600 m in elevation) based on whether bedrock crops out. The bedrock outcrop section is the source area, and the section buried in colluvium is the transitional area.

### 5.1.1 Source area

The source area in this section mainly refers to bedrock exposures whose elevation is 1600–1890 m. The slope gradient varies from  $50^{\circ} - 75^{\circ}$ . The source area can be divided into two sub-source I and sub-source II (Fig. 13).

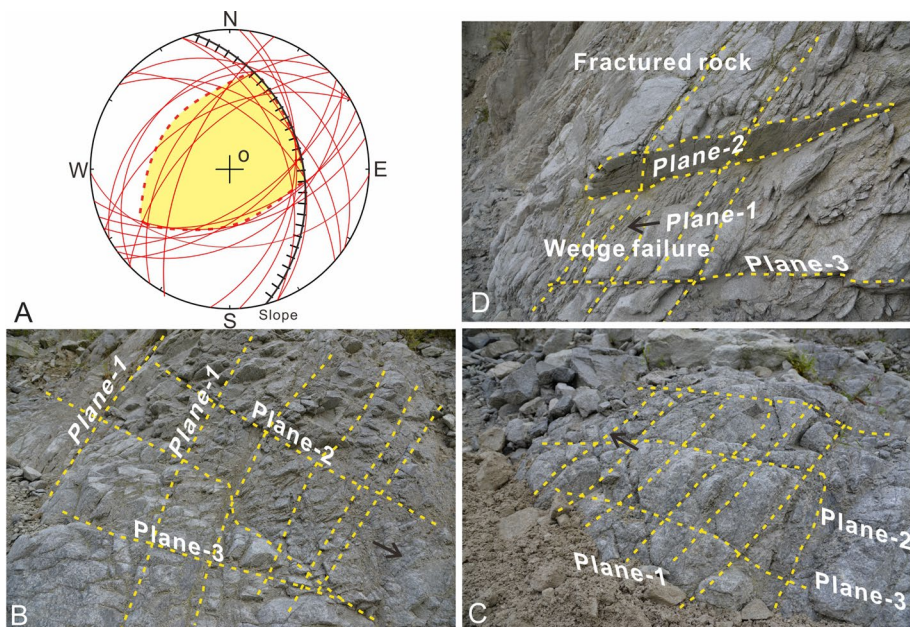


**Fig. 12** Stereographic project diagram in source zone (a) and typical wedge rock masses (b, c) and wedge failures in source zone (d). Locations of b, c and d are listed in Fig. 13a

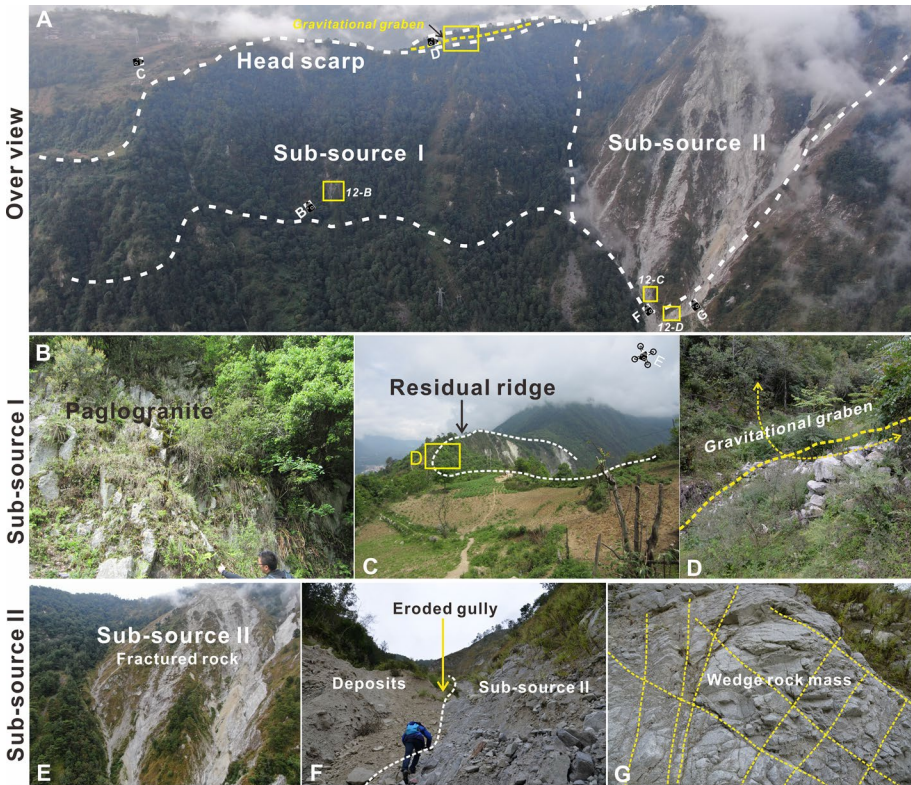


**Fig. 13** Typical characteristics of source zone. **a** Overall view of source area, **b** bedrock in sub-source I, **c** narrow ridge (head scarp), **d** gravitational graben in narrow ridge, **e** overall view of sub-source II, **f** eroded gully is developed in the boundary of bedrock and deposit, **g** fractured rocks and wedge failure in source area

Sub-source I is located in the southern section of the source area and is a relatively stable area; outcrops of plagiogranite generally cover this sub-zone (Fig. 13b). The slope gradient is generally between 50° and 60°, and obvious gravitational grabens are found in this sub-zone (Figs. 11, 13d). The headscarp is a typical narrow ridge (Fig. 13c). Some eroded gullies are also present.

Sub-source II is located in the northern section of the source area; it is in an unstable state at present, the rocks are fractured, and rock falls occur frequently (Fig. 13e). An eroded gully has developed in the boundary between sub-source II and the deposits (Fig. 13f). A detailed field investigation shows that the bedrock is very fractured, and fractures cut the rocks into wedge-shaped masses (Fig. 13g).

### 5.1.2 Transitional area

The transitional area is the transition zone between the source area and the deposit zone (Figs. 11, 14a). The elevation of this area varies from 1380 to 1600 m, and the slope gradient is approximately 30°–40°, which is obviously less than that of the source area.

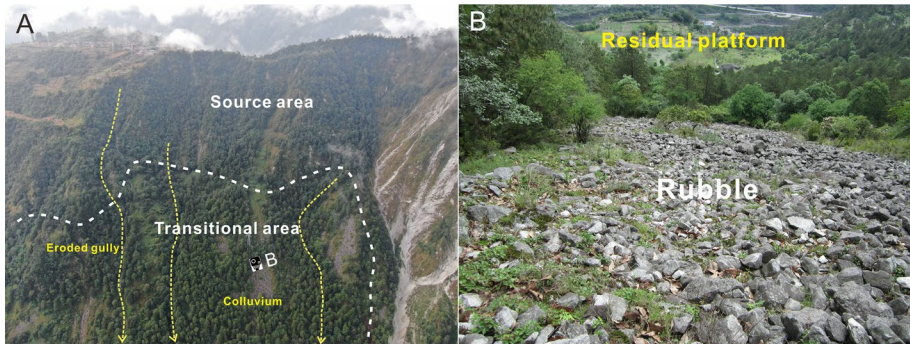


**Fig. 14** Images show typical features of Transition zone. **a** UAV image shows overall view of transition zone, **b** rubbles (colluvium) cover on the transition zone

The surficial deposits are colluvium that is composed of rubble and blocks whose sizes are mainly concentrated at 5–15 cm (gravel) and 15–28 cm (blocks) (Fig. 14b), while its bedrock forms part of the source area (Fig. 10). The surficial deposits mainly originated from later rock falls after the MGL event, and rock falls continue to occur frequently. Some prominent deeply eroded (5–10 m) gullies are found in this area.

## 5.2 Deposit zone

According to the morphological elements and geological structures, the deposit zone can be divided into sub-deposit I and sub-deposit II.

### 5.2.1 Sub-deposit zone I

This sub-deposit zone is the main body of the MGL deposit and is mainly concentrated at elevations of 1120–380 m. Due to Dadu River erosion, sub-source zone I can be divided into a left bank deposit and a right bank deposit (Figs. 11, 15b).

The right bank deposit is the main deposit and contains a deposit platform (Figs. 11, 15a). The deeply eroded gully (depth: 50 m) cuts the deposit platform into two parts (platform 1 and platform 2), as shown in Fig. 15a. The elevations of these two platforms vary mainly from 1330 to 1380 m, and the slope gradient is gentle ( $5^{\circ}$ – $10^{\circ}$ ). The front section of the right bank deposit is a steep slope whose gradient and height are approximately  $50^{\circ}$  and 210 m, respectively, and a clear local scarp is present (Fig. 15d), indicating that the right bank deposit has been intensely eroded.

The field investigation shows that some landslide deposits with the same contents as in the right bank deposit are also found on the left bank of the Dadu River (Fig. 15b, e). These left bank deposits are distributed above the river and extend to the road (Fig. 15c). The colluvium consisting of the Triassic Xujiahe Group that comes from the left bank mountain partially covers the MGL deposit (Fig. 15f, g). This situation indicates that the MGL dam may have been higher than the current road elevation (approximately 1150 m). The MGL can be concluded to have blocked the Dadu River, and the dam height was at least 30 m (the Dadu River level is 1120 m).



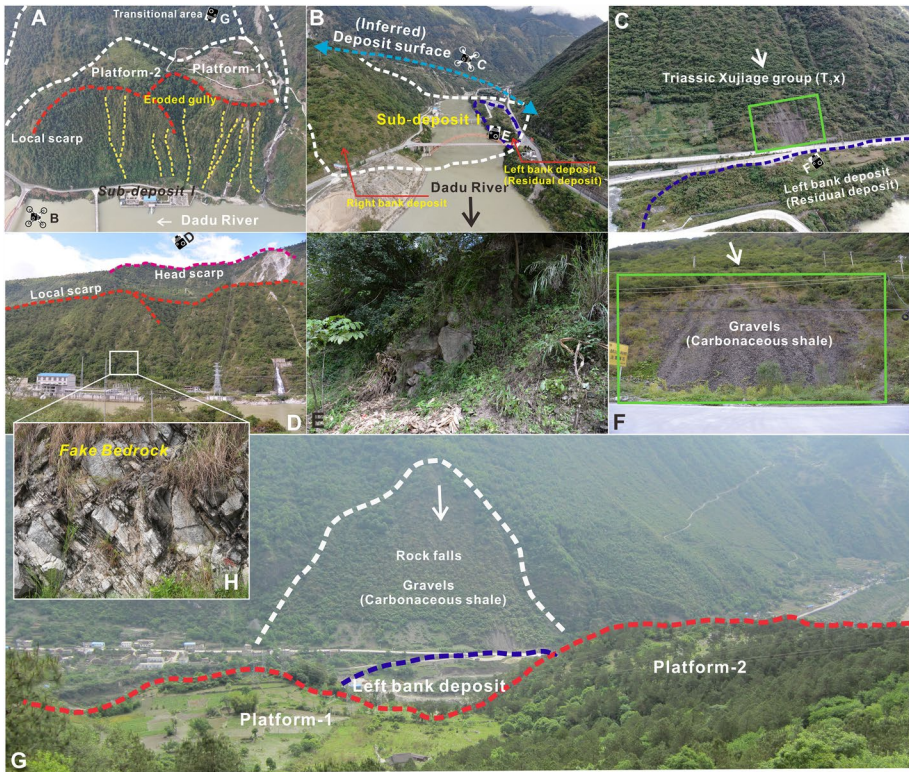


**Fig. 15** Images show the typical characteristics of sub-deposit I. **a** Overall view of sub-deposit I, **b** deposits are eroded into two sections by Dadu River, **c** gravels (carbonaceous shale) lie on the deposit that from the Triassic Xujiahe Group (right bank), **d**, **e** show local typical features of deposits; **f** shows detail features of left bank rock falls (carbonaceous shale); **g** shows features of platforms, left bank deposit and left bank rock falls (colluvium)

### 5.2.2 Sub-deposit zone II

Sub-deposit zone II presents an irregular triangular shape (Fig. 16a); the deposits in this zone mainly consist of soils and gravels belonging to unconsolidated deposits. There is only one erosion gully in this zone whose length and profile slope are 770 m and 20°, and it is very active that the debris flows occur almost every years according to local reports (Fig. 16b). At present, this gully has been eroded intensely, and its depths reach 10–14 m (downstream), 16–20 m (middle stream) and 10–13 m (upstream), as shown in Fig. 16c, d, e, f, g.

The catchment area of this zone is located in sub-source II with an area of  $17 \times 10^4 \text{ m}^2$ . The average annual rainfall for the MGL area (Luding station) listed in Table 3 reveals that intense rainfall is concentrated mainly in the summer season (June–September) and that the maximum daily rainfall reaches 72 mm. These conditions provide sufficient flood waters for the occurrence of debris flows. After the occurrence of a strong debris flow (one that erodes deeply), the gully bank frequently collapses (Fig. 16c, d, e, f, g) because the slope foot has been eroded, which prepares the provenance for the next debris flow. The erosion cycle is summarized in Fig. 16h, and every cycle makes the gully eroded wider and deeper.

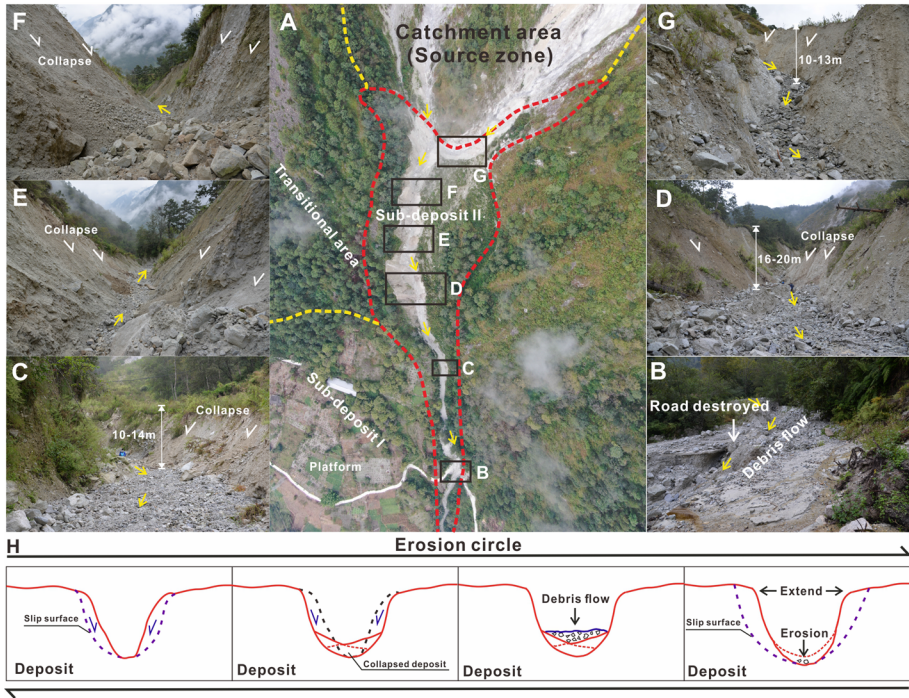


**Fig. 16** Images and concept maps show the typical characteristics of sub-deposit II. **a-** The UAV image shows the overall view of sub-deposit II; **b, c, d, e, f, g** the field images show the detail characteristics of sub-deposit II; **h** the erosion circle of deposits

**Table 3** Rainfall data (multi-annual average: 1952–2008) for the MGL area (Luding station) (Wu 2013)

Average	Jan	Feb	Mar	Apr	May	June	July	Aug	Sep	Oct	Nov	Dec	mm
Monthly	0.9	3.2	15.9	36.8	65.6	105.1	143.0	145.7	85.1	33.3	7.9	0.6	Total 642.9
Max. daily	4.2	8.4	13.3	20.7	30.2	67.6	72.3	65.9	61.8	45.0	17.7	3.6	Max 72.3

## 6 Discussion

### 6.1 Failure mechanism

#### 6.1.1 Deterioration by multiple factors

Prior to the Moxi earthquake-triggered MGL, the rock mass in the source zone had been unstable, and a good indicator is that outcrops of very fractured rocks are still present and collapse frequently in the source area (sub-source II) and on MGL Mountain, as shown in Figs. 4, 12 and 13. This shattering is the cumulative result of numerous adverse geological

factors, such as high geostress and intense unloading, an active fault (Detuo fault), concave erosion and frequent earthquakes.

**6.1.1.1 High geostress and intense unloading.** As noted in Sect. 2.1, the MGL area is located at the intersection of two fault zones: the Xianshuihe fault zone and the Longmenshan fault zone (Fig. 1b). The construction of a nearby power station (Dagangshan station) reveals that the core diskling phenomenon is very common during drilling, and in situ tests show that the maximum principal stress reaches 26 MPa in the direction of  $N50^{\circ}-75^{\circ}W$ . These characteristics imply that the MGL area is an area with high geostress and that its direction is approximately perpendicular to the river trend and the ridge line of MGL Mountain.

Rapid river erosion (0.38 mm/y, Zhao et al. 2013) has generated a deeply cut canyon along the Dadu River (V-shaped valley). During this process, strong unloading has occurred in the granite body with high energy storage, and numerous unloading fissures have been produced, especially in the MGL area, because its direction is perpendicular to the direction of high geostress.

**6.1.1.2 The Detuo fault** As shown in Figs. 8, 17, the Detuo fault just crosses the slope foot. The scanning electron microscopy (SEM) and electron spin resonance (ESR) dating of Detuo fault gouges shows that from  $N_1$  (middle Neogene) to  $Q_1$  (Quaternary), the activity on the Detuo fault increased; it peaked at  $Q_1$  and then began to decrease continuously. The latest activity is recorded mainly by  $Q_1-Q_3$ , with no obvious activity since  $Q_3$  (Cai et al. 2013). The movements along the Detuo fault fractured the rock mass continuously over a long time scale.

**6.1.1.3 Strong erosion at the cut bank** The interpreted results of the geophysical prospecting profile (Fig. 8) and the drill holes (Fig. 10) indicate that the current course of the Dadu River was diverted, forced by the MGL; the original channel followed the slope foot, and the MGL is located in the cut bank (concave bank) of the Dadu River. The continuous lateral scouring of the slope foot in the cut bank eroded the rock mass, which weakened the integrity of the rock mass and contributed to the occurrence of the MGL.

**6.1.1.4 Frequent earthquakes** As noted in Sect. 2, the MGL area is an earthquake-prone region (Fig. 1), and many large earthquakes have occurred near the MGL, such as the recent 2013 Lushan M 7.0 earthquake and the 2014 Kangding M 6.3 earthquake (Zhao 2020). The frequent large earthquakes enhanced the structural planes, especially in the source area of the MGL, which is a typical narrow ridge (Fig. 17) with a very strong site effect (discussed in detail in Sect. 6.1.2). The integrity of the rock mass in the source area has been weakened continuously during earthquakes.

These processes caused the structural planes to penetrate throughout the source area and greatly reduced its stability. The field investigations show that numerous structural planes cut the rock mass into wedge-shaped masses.

## 6.1.2 Strong earthquake coupled with site effects triggered the MGL

Although the MGL is not located in the highest intensity area, the landslide occurred in this place. An important factor is the site amplification effect that could be responsible for this event. The site amplification effect implies that different geomorphic units

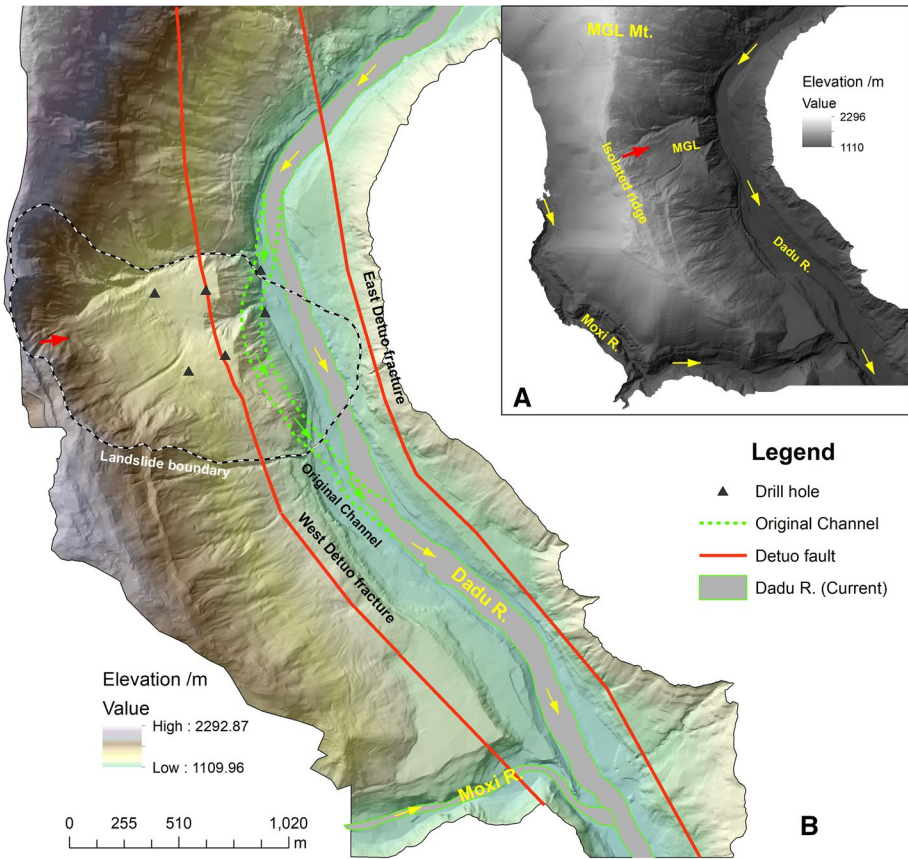


**Fig. 17** Characteristics of Mogangling Mountain and Dadu River. **a** Topographic features MGL mountain, **b** Dadu River diversion and position of Detuo fault

and elevations can produce different dynamic responses to basic seismic shaking (Fiore 2010; Wang et al. 2017).

On 20 April 2013, an M 7.0 earthquake (Lushan earthquake) occurred in the Longmenshan fault zone (Fig. 1), whose distance to the Lengzhuguan station is approximately 86 km (Fig. 6). The Lengzhuguan station recorded this earthquake, and Table 4 and Fig. 18 show the typical seismic parameters for different accelerometers during the Lushan earthquake.

**Table 4** Basic seismic parameters of Lushan earthquake

Accelerometer	PGA ( $m \times s^{-2}$ )			Elevation (m)
	NS	EW	UD	
L1	1.538	1.635	0.667	1516
L2	0.393	0.424	0.290	1478
L7R (Reference station)	0.139	0.126	0.111	1686

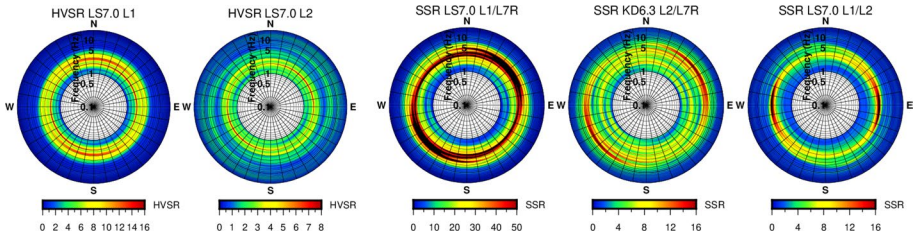


**Fig. 18** Polar diagrams of D-HVSR (horizontal-to-vertical spectral ratios) and D-SSR (standard spectral ratios) of Sites L1 and L2

From Table 4 and Fig. 18, the narrow ridge (L1 and L2) experienced stronger site amplification than the large mountain (L7R), although the elevation of the mountain is higher than that of the narrow ridge; the amplification factor reached 2.6–13.0 peak ground acceleration (PGA, Table 4) and 16–50 standard spectral ratio (SSR, Fig. 18). For the narrow ridge, the PGA of the ridge top reached 1.6 m/s<sup>2</sup> (EW), 1.5 m/s<sup>2</sup> (NS) and 0.7 m/s<sup>2</sup> (UD), which provided overall directional site amplification and could produce more obvious amplification than in the lower part; the amplitudes could reach 10 and perhaps more (Fig. 18). The site resonances of sites L1 and L2 ranged between frequencies of 2 and 5 Hz, especially near 2 Hz (Fig. 18).

From the above analysis, the narrow ridge produced stronger site amplification than the large mountain, especially at the ridge top whose PGA exceeded 1.6 m/s<sup>2</sup> (EW), although the Lushan earthquake magnitude was only 7.0 and the distance was greater than 80 km. Actually, the seismic conditions at the MGL site should have been much stronger during the Moxi earthquake because the magnitude of the Moxi earthquake was 7.75, and the distance to the seismic fault was only 2 km. As a reference, the Qingping national seismic station (China), located on a stable rock mass, successfully recorded the 2008 Wenchuan M 8.0 earthquake, and its distance to the seismic fault (Yingxiu–Beichuan fault) is approximately 3.0 km. The PGA of the Wenchuan earthquake at Qingping station reached 8.2 m/s<sup>2</sup> (EW), 8.0 m/s<sup>2</sup> (NS) and 6.2 m/s<sup>2</sup> (UD) (Liu and Li 2012). Therefore, we estimate that the PGA of the MGL source area (isolated ridge top) should have exceeded 1 g considering site amplification, and the MGL could easily have occurred under this seismic condition.

The failure process of the MGL can be summarized in four phases, as shown in Fig. 19. (1) Rapid erosion by the Dadu River and the Moxi River carved part of MGL Mountain into a narrow ridge, especially in the source area (Fig. 19a). During this process, unloading caused the granite, which can store high energy, to produce numerous unloading fissures, and frequent earthquakes extended these fissures and weakened the integrity of the rock mass. (2) With continuous erosion, the Detuo fault produced plastic deformation, which potentially destabilized the rock mass (Fig. 19b). (3) The 1786 Moxi M 7.75 earthquake coupled with the site amplification effect and all the penetrating structural planes led to the occurrence of the MGL. The landslide dam blocked the Dadu River (Fig. 19c). (4) Ten days after the landslide blocked the Dadu River, the dam broke, and the current topographic features formed after hundreds of years of erosion (Fig. 19d).

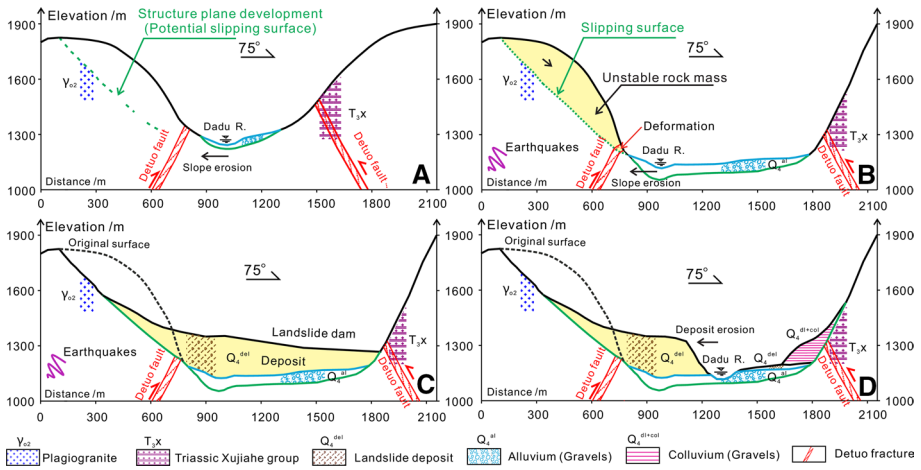


**Fig. 19** Failure process of MGL landslide. **a** Concave incision erodes slope foot continuously, **b** Detuo fault deteriorated the slope stability further, **c** MGL landslide was triggered by Moxi earthquake and blocked the Dadu River, **d** long-term river erosion formed current topography

### 6.2 The dammed lake

After the occurrence of the MGL, a landslide dam blocked the Dadu River. The elevation of the left bank deposit is approximately 1150 m. However, the elevations of the residual deposit platform (1330–1380 m) and the completely accumulated deposit indicate that the elevation of the left bank deposit at that time may have exceeded the current value of 1150 m.

For a landslide, the lowest elevation of a deposit is generally at the toe of the deposit, and the dammed lake water also overflows the landslide dam at the lowest elevation of the deposit. Therefore, estimating the elevation of the left bank deposit by calculating the volume of the dammed lake could be a good idea and valuable historical records may help accomplish this task.

The average flow along the Luding section of the Dadu River varies from 100–1500 m<sup>3</sup>/s, and the annual average flow (1952–2008) is 891 m<sup>3</sup>/s. The landslide occurred on 1 June, when the upstream Dadu River was experiencing the rainy season (Table 3). According to the suggested average flow at the nearby power station (Luding station), a value of 1100 m<sup>3</sup>/s is adopted to estimate the volume of the dammed lake approximately.

According to historical records, the landslide dam held for ten days, and the volume of the dammed lake was 1100 × 60 × 60 × 24 × 10 = 9.504 × 10<sup>8</sup> m<sup>3</sup>. Based on the ArcGIS platform, digital elevation model (DEM) data with a resolution of 12.5 m are used to invert the elevation level of the dammed lake according to its volume, and the results show that the elevation level of the dammed lake was 1250 m, and the dammed lake area was approximately 19.91 km<sup>2</sup>. These numbers indicate that the elevation of the deposit toe could have reached 1250 m, which is 130 m higher than the current river level. The dammed lake extended approximately 31.4 km, and the towns of Jiajun and Lengqi were both seriously damaged by the lake waters, as shown in Fig. 20a, which coincides with local descriptions.

Ten days after the occurrence of the MGL, the landslide dam broke (Fig. 20b), in order to acquire the peak flow of a dam break, a regression model proposed by Peng and Zhang (2012) is adopted.

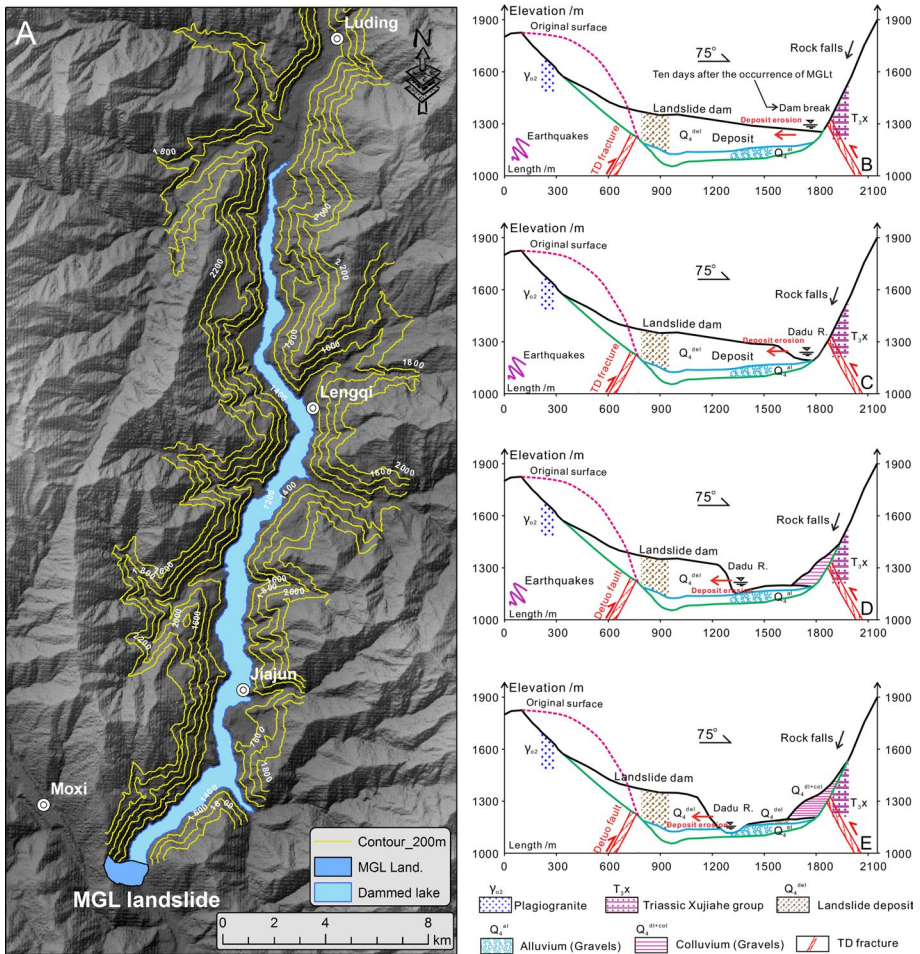


**Fig. 20** Dam Lake and dam erosion evolution process. **a** Dammed lake distribution after MGL landslide, **b** dam broke ten days after the occurrence of MGL landslide, **c, d, e** landslide dam erosion evolution process with time going

$$\frac{Q_p}{g^{1/2}H_d^{5/2}} = \left(\frac{H_d}{H_r}\right)^{-1.417} \left(\frac{H_d}{W_d}\right)^{-0.265} \left(\frac{V_d^{1/3}}{H_d}\right)^{-0.471} \left(\frac{V_l^{1/3}}{H_d}\right)^{1.569} e^\alpha \quad (2)$$

where  $Q_p$  is the peak flow,  $H_d$  is the dam height,  $W_d$  is the dam width (the base width of the landslide dam measured parallel to the main valley axis, Peng and Zhang 2012),  $V_d$  is the dam volume,  $V_l$  is the lake volume,  $H_r$  is a reference height (1 m, Wu et al. 2020),  $g$  is gravity and  $\alpha$  represents the erodibility of the dam. For the parameters of this dam break,  $H_d=130$  m (130 m=deposit elevation: 1250 m—river elevation: 1120 m),  $W_d=700$  m,  $V_d=2500 \times 10^4$  m<sup>3</sup>, and  $V_l=9.504 \times 10^8$  m<sup>3</sup>. Because the deposits are mostly fractured blocks and the erodibility of the dam can be treated as moderate,  $\alpha$  is set to  $-0.336$  (Peng and Zhang 2012). After calculation, the peak flow  $Q_p \geq 7100$  m<sup>3</sup>/s.

The outburst flood rushed downstream, and more than 100 000 people in the downstream reach lost their lives during this flood according to historical records. Loosened landslide deposits were also eroded rapidly from the deposit toe (Fig. 20c). Because the MGL is located on a concave bank of the Dadu River, concave bank erosion makes the river channel migrate gradually towards the right. As a result of this process, frequent rock falls on the left bank have partially covered the residual deposit, and a steep slope ( $> 60^\circ$ ) has formed in the eroded deposit on the right bank (Figs. 20d, e). The landslide dam erosion process is shown in Fig. 20.

## 7 Conclusion

At noon, 1 June 1786, the Moxi M 7.75 earthquake struck the MGL area and triggered the MGL; the distance from its source area to the seismogenic fault was approximately 2 km, and the seismic intensity was degree IX. The MGL blocked the Dadu River for ten days and caused more than 100 000 deaths after the landslide dam was breached.

The source area of the MGL is located at the intersection of the Xianshuhe fault zone and the Longmenshan fault zone. The regional high geostress, the rapid river erosion and an active fault (Detuo fault) that just crosses the slope foot have led to fractures in the rock mass in the source area, which cut the rock mass into wedges.

The MGL occurred on a narrow ridge that can produce a strong site amplification effect, and the seismic response to the 2013 Lushan M 7.0 earthquake indicates that shaking of the isolated ridge can be magnified 10 times or more compared with that of the large mountain, especially at the top part of the narrow ridge. The basic seismic conditions provided by the Moxi earthquake and the superimposed site amplification effect supplied enough seismic shaking energy for the occurrence of the MGL.

The MGL dammed the Dadu River, and during the ten days of river blockage, the volume of the dammed lake reached  $9.504 \times 10^8 \text{ m}^3$  with an area of  $19.91 \text{ km}^2$  and a water level of 1250 m, approximately 130 m higher than the current river level.

**Acknowledgements** This study was supported by the National Natural Science Foundation of China (Grant No. 41877235, 42007273), the National Key Research and Development Program of China (Grant No. 2017YFC1501000), the National Science Funds for Creative Research Groups of China (Grant No. 41521002) and the China Postdoctoral Science Foundation (2020M673292). The authors express their gratitude for this financial assistance.

## Compliance with ethical standards

**Conflict of interest** The authors declare that they have no conflict of interest.

## References

- Antinao JL, Gosse J (2009) Large rockslides in the southern central Andes of Chile ( $32\text{--}34.5^\circ\text{S}$ ): tectonic control and significance for quaternary landscape evolution. *Geomorphology* 104:117–133
- Cai XL, Wu DC, Wang DY (2013) SEM analysis of quartz gravel surface in gouge of Detuo fault zone. *J Yangtze Univ* 10(26):45–49 ((In Chinese with English abstract))
- Chen J, Dai F, Lv T, Cui Z (2013) Holocene landslide-dammed lake deposits in the upper Jinsha river, SE Tibetan plateau and their ages. *Quatern Int* 298:107–113



- CIGMR (Chengdu Institute of Geology and Mineral Resources) (1975) Geological map of Xingjing County (1:200000). Map No. H-48-XIX. (in chinese)
- Cui P, Dang C, Zhuang JQ, You Y, Chen XQ, Scott KM (2012) Landslide-dammed lake at Tangjiashan, Sichuan province, China (triggered by the Wenchuan earthquake, May 12, 2008): risk assessment, mitigation strategy, and lessons learned. *Environ Earth Sci* 65(4):1055–1065
- Dai F, Lee C, Deng J, Tham L (2005) The 1786 earthquake-triggered landslide dam and subsequent dam-break flood on the Dadu River Southwestern China. *Geomorphology* 73(3):277–278
- Deng H, Wu LZ, Huang RQ, Guo XG, He Q (2017) Formation of the Siwanli ancient landslide in the Dadu River. *China Landslides* 14(1):385–394
- Fiore VD (2010) Seismic site amplification induced by topographic irregularity: results of a numerical analysis on 2d synthetic models. *Eng Geol* 114(3–4):109–115
- Gorum T, Fan X, Van Westen CJ, Huang RQ, Xu Q, Tang C, Wang G (2011) Distribution pattern of earthquake-induced landslides triggered by the 12 May 2008 Wenchuan earthquake. *Geomorphology* 133(3–4):152–167
- Gu J, Wang YS, Cao WZ, Zhang L, Huang JL, He JX, Liu Y (2016) Formation mechanism and motion process of Lantianwan landslide triggered by the 1786 Moxi earthquake. *Mountain research*. (in chinese with english abstract)
- Guo C, Zhan Y, Montgomery DR (2016) How unusual is the long-runout of the earthquake-triggered giant Luanshibao landslide, Tibetan Plateau, China? *Geomorphology* 259:145–154
- Havenith HB (2014) Hazard and risk related to earthquake-triggered landslide events. Springer International Publishing, *Landslide Science for a Safer Geoenvironment*
- Hewitt K, Clague J, Orwin JF (2008) Legacies of catastrophic rock slope failures in mountain landscapes. *Earth Sci Rev* 87:1–38
- Hubbard J, Shaw JH (2009) Uplift of the Longmen Shan and Tibetan plateau, and the 2008 Wenchuan (M= 7.9) earthquake. *Nature* 458(7235):194–197
- Huang RQ, Fan XM (2013) The landslide story. *Nat Geosci* 6(5):325
- Huang RQ, Pei XJ, Fan XM, Zhang WF, Li SG, Li BL (2012) The characteristics and failure mechanism of the largest landslide triggered by the Wenchuan earthquake, May 12, 2008. *China Landslides* 9(1):131–142
- Huang R, Wang Y, Wang S, Li Y (2011) High geo-stress distribution and high geo-stress concentration area models for eastern margin of Qinghai-Tibet plateau. *Sci China Technol Sci* 54(1):154–166
- Kargel S, Leonard GJ, Shugar DH, Haritashya UK (2016) Geomorphic and geologic controls of geohazards induced by Nepal's 2015 Gorkha earthquake. *Science* 351(6269):140–151
- Korup O, Clague JJ, Hermanns RL, Hewitt K, Strom AL, Weidinger JT (2007) Giant landslides, topography and erosion. *Earth Planet Sci Lett* 261:578–589
- Liu L (2014) Application of audio magnetotelluric sounding in the geothermal field. Chengdu University of Technology. Master thesis. (in chinese with english abstract)
- Liu L, Li XJ (2012) Peak ground acceleration attenuation relationship of Wenchuan 8.0 earthquake. *J Beijing Univ Technol* 38(2):173–179 **(In Chinese with English abstract)**
- Nanson GC, Hickin EJ (1986) A statistical analysis of bank erosion and channel migration in western Canada. *Geol Soc Am Bull* 97(4):497–504
- Page K, Nanson G (1982) Concave-bank benches and associated floodplain formation. *Earth Surf Proc Land* 7(6):529–543
- Pánek T, Hradecký J, Smolková V, Šilhán K, Minár J, Zernitskaya V (2010) The largest prehistoric landslide in northwestern Slovakia: chronological constraints of the Kykula long-runout landslide and related dammed lakes. *Geomorphology* 120(3–4):233–247
- Papadimitriou E, Wen X, Karakostas V, Jin X (2004) Earthquake triggering along the Xianshuihe fault zone of western Sichuan. *China Pure Appl Geophys* 161(8):1683–1707
- Peng M, Zhang LM (2012) Breaching parameters of landslide dams. *Landslides* 9(1):13–31
- Petley DN (2013) Characterizing giant landslides. *Science* 339(6126):1395–1396
- Qi JH, Xu M, An CJ, Wu ML, Zhang YH, Li X (2017) Characterizations of geothermal springs along the Moxi deep fault in the western Sichuan Plateau, China. *Phys Earth Planet Inter* 263:12–22
- Ren J, Xu X, Zhang S, Yeats RS, Chen J, Zhu A, Liu S (2018) Surface rupture of the 1933 M 7.5 Diexi earthquake in eastern Tibet: implications for seismogenic tectonics. *Geophys J Int* 212(3):1627–1644
- Sun JB, Yue H, Shen ZG, Fang LH, Zhan Y, Sun XY (2018) 2017 Jiuzhaigou earthquake: a complicated event occurred in a young fault system. *Geophys Res Lett* 45:1–12
- Turnbull JM, Davies TR (2006) A mass movement origin for cirques. *Earth Surf Proc Land* 31:1129–1148

- Wang Z, Wang J, Chen ZL, Liu YP, Huang RQ, Pei SP (2011) Seismic imaging, crustal stress and gps data analyses: implications for the generation of the 2008 Wenchuan earthquake (M7.9) China. *Ondwana Res* 19(1):202–212
- Wang XM, Pei XY (1988) The 1786 Kangding-Luding earthquake. *Earthquake research in Sichuan*, 1–51. (in chinese with english abstract)
- Wang YF, Cheng QG, Lin QW (2018a) Insights into the kinematics and dynamics of the Luanshibao rock avalanche (Tibetan Plateau, China) based on its complex surface landforms. *Geomorphology* 317:170–183
- Wang YS, Li WG, Huang RQ, Luo YH (2007) The unloaded and relaxed phenomena in the valley bottom of the Daduhe River and its genetic mechanism. *J Chengdu Univ Technol* 34(4):379–383 (**in chinese with english abstract**)
- Wang YS, He JX, Luo YH (2017) Seismic response of the Lengzhuguan slope during Kangding Ms58 earthquake. *J Mt Sc* 14(11):2337–2347
- Wang Y, Zhao B, Li J (2018b) Mechanism of the catastrophic june 2017 landslide at Xinmo village, Songping river, Sichuan province China. *Landslides* 15(2):333–345
- Wang Y, Wu LZ, Gu J (2019) Process analysis of the Moxi earthquake-induced Lantianwan landslide in the Dadu River, China. *Bull Eng Geol Env* 78(7):4731–4742
- Wang YS, Wu JF, Luo YH, Xiao M, Shun L, Qing Q (2012) Seismic landslides and the environmental impact in the middle reach of Daduhe river. *Adv Mater Res* 368:1965–1970
- Wu JF 2013 Research on development characteristics and genetic mechanism of the seismic landslide in Dadu River Chengdu University of Technology, Ph D thesis (in chinese with english abstract)
- Wu JF, Wang YS, Luo YH (2011) The characteristics and mechanism of large scale landslides between Huangjinping and Detuo in Daduhe river. *Adv Mater Res* 243:3211–3216
- Wu LZ, Deng H, Huang RQ (2018) Evolution of lakes created by landslide dams and the role of dam erosion: a case study of the Jiajun landslide on the Dadu River, China. *Quatern Int* 503:41–50
- Wu LZ, Zhao DJ, Zhu JD, Peng JB, Zhou Y (2020) A Late Pleistocene river-damming landslide, Minjiang River. *China Landslides* 17(2):433–444
- Yang CM, Yu WL, Dong JJ, Kuo CY, Shimamoto T, Lee CT (2014) Initiation, movement, and run-out of the giant Tsaoling landslide—what can we learn from a simple rigid block model and a velocity–displacement dependent friction law? *Eng Geol* 182:158–181
- Xu Q, Fan XM, Huang RQ, Van Westen C (2009a) Landslide dams triggered by the Wenchuan Earthquake, Sichuan Province, south west China. *Bull Eng Geol Env* 68(3):373–386
- Xu Q, Zhang S, Li WL (2011) Spatial distribution of large-scale landslides induced by the 5.12 wenchuan earthquake. *J Mt Sci* 02:146–160
- Xu WJ, Xu Q, Wang YJ (2013a) The mechanism of high-speed motion and damming of the Tangjiashan landslide. *Eng Geol* 157:8–20
- Xu X, Gao R, Guo X, Li W, Li H, Wang H, Lu Z (2017) Outlining tectonic inheritance and construction of the Min Shan region, eastern Tibet, using crustal geometry. *Sci Rep* 7(1):1–8
- Xu X, Wen X, Yu G, Chen G, Klinger Y, Hubbard J, Shaw J (2009b) Coseismic reverse-and oblique-slip surface faulting generated by the 2008 Mw 7.9 Wenchuan earthquake China. *Geology* 37(6):515–518
- Xu X, Wen X, Han Z, Chen G, Li C, Zheng W, Wei Z (2013b) Lushan M S 70 earthquake: a blind reserve-fault event. *Chin Sci Bull* 58(28–29):3437–3443
- Yin YP, Li B, Wang WP (2015) Dynamic analysis of the stabilized Wangjiayan landslide in the wenchuan ms 8.0 earthquake and aftershocks. *Landslides* 12(3):537–547
- Zhang J (2015) Application study on geological exploration to deeply-buried highway tunnel with V8 multifunctional electrical workstation in Guangxi Province. Guangxi University, master thesis. (in chinese with english abstract)
- Zhao B (2020) The Mechanism of Large Earthquake-Triggered Landslides in Area of High Intensity and Deep Canyon of Northwest Sichuan. Chengdu University of Technology. Ph.D thesis. (in chinese with english abstract)
- Zhao B, Huang Y, Zhang C, Wang W, Tan K, Du R (2015) Crustal deformation on the Chinese mainland during 1998–2004 based on GPS data. *Geod Geodyn* 6:7–15
- Zhao B, Li W, Wang Y, Lu J, Li X (2019) Landslides triggered by the Ms 6.9 Nyingchi earthquake, China (18 November 2017 analysis of the spatial distribution and occurrence factors. *Landslides* 16(4):765–776
- Zhao GZ, Unsworth MJ, Zhan Y, Wang LF, Zhang JH (2012) Crustal structure and rheology of the Longmenshan and Wenchuan mw 79 earthquake epicentral area from magnetotelluric data. *Geology* 40(12):1139–1142

- Zhao ZJ, Liu Y, Chen Y, Zhang MH, Shu Q (2013) Quaternary fluvial incision rates of the western Sichuan plateau inferred from ESR chronology. *J Lanzhou Univ* 49(2):160–167 **((in chinese with english abstract))**
- Zhou H, Liu HL, Kanamori H (1983) Source processes of large earthquakes along the Xianshuihe fault in southwestern China. *Bull Seismol Soc Am* 73(2):537–551
- Zhou RJ, He YL, Huang ZZ, Li XG, Yang T (2001) The slip rate and strong earthquake recurrence interval on the Qianning-Kangding segment of the Xianshuihe fault zone. *Acta Seismol Sin* 23:250–261 **((in chinese with english abstract))**

**Publisher's Note** Springer Nature remains neutral with regard to jurisdictional claims in published maps and institutional affiliations.